Yoon et al. *NPG Asia Materials* (2020) 12:16
https://doi.org/10.1038/s41427-020-0198-7

NPG Asia Materials

ARTICLE Open Access

Selective growth of α-form zinc phthalocyanine nanowire crystals via the flow rate control of physical vapor transport

Youngkwan Yoon[1], Soyoung Kim[1] and Hee Cheul Choi[1]

Abstract

α-Form zinc phthalocyanine (ZnPc), a kinetically favorable form of ZnPc, is an efficient photosensitizer for photodynamic cancer therapy, especially when it is formed into nanowires (NWs), which have high water dispersibility. To take full advantage of this material, it is necessary to selectively grow kinetically favorable α-form ZnPc NWs over thermodynamically favorable β-form ZnPc NWs. The present study reports the selective growth of kinetically favorable α-form ZnPc NW crystals by a physical vapor transport method with flow rate control of the carrier gas. The flow rate is key for the dominant growth of α-form ZnPc NWs, thus enabling control of the crystal size, which critically affects the stability of ZnPc crystals. The yield of α-form ZnPc NWs was over 98% at a flow rate of 2000 sccm of Ar carrier gas. This approach could be applied for various Pc molecules, including copper phthalocyanine (CuPc). Our findings might contribute to the development of novel strategies for the selective growth of high-quality kinetically favorable crystals with a specific structure and provide great opportunities for their various practical applications.

Introduction

Kinetically favorable metastable crystals frequently exhibit remarkable properties superior to those of their thermodynamically favorable and more stable products.[1–7] Therefore, the selective growth of the desired crystals, especially in kinetically favorable structures, is an important issue not only for the fundamental study of the crystal growth mechanism but also for their practical applications. However, such specific crystal structure control is difficult because it is normally determined by thermodynamic equilibrium and influenced by various crystallization conditions that affect not only thermodynamic but also kinetic controls.[4,8–12] Therefore, polymorphism is quite commonly observed, especially in organic and organometallic molecular crystals, due to their various weak nondirectional intermolecular van der Waals forces.[4,13–15] Polymorph crystals having kinetically and thermodynamically favorable structures show significantly different properties depending on the stacking structure. For example, the metastable α-phase of 2,6-dichloronaphthalene diimide exhibits much higher mobility than the stable β-phase due to their different electronic couplings between neighboring molecules.[4,5] Additionally, metastable Y-form titanyl phthalocyanine shows a photogeneration quantum yield greater than 90%, which is much higher than those of the stable α- and β-forms.[2,6,7] To date, there have been many trials to control the crystal morphology and structure via various strategies without suggestion of a facile strategy for obtaining such kinetically favorable structure-controlled crystals.

Previously, our group reported α-form ZnPc nanowires (NWs) that showed substantially improved water dispersibility and highly efficient dual photodynamic and photothermal performances, both of which have a synergistic effect in cancer phototherapy, as demonstrated by both in vitro and in vivo tests.[3] However, the difficult phase separation of simultaneously obtained kinetically favorable α-form and thermodynamically favorable

Correspondence: Hee Cheul Choi (choihc@postech.edu)
[1]Department of Chemistry, Pohang University of Science and Technology (POSTECH), 77 Cheongam-ro, Nam-gu, Pohang-si 37673, Korea

β-form ZnPcs still remains a major limitation in the practical usage of this material as an anticancer agent because the presence of a small amount of β-form ZnPc causes aggregation and precipitation in solution. Therefore, the selective growth of high-quality and high-yield kinetically favorable α-form ZnPc NWs is an important and urgent issue for practical applications, including clinical tests. Herein, we focused on the development of a facile and efficient method for the selective growth of α-form ZnPc NWs and found that the flow rate control of carrier gas during the physical vapor transport (PVT) process could induce the dominant growth of kinetically favorable α-form ZnPc NWs. From various studies on Pc, it is well known that the crystal phase is highly related to the crystal size regardless of the growth method.[16–20] Control of the crystal size during solution-phase crystallization is difficult without using additional chemicals such as capping reagents and surfactants. Therefore, we used the PVT method, a vapor-phase crystallization method that is appropriate to obtain pure and high-quality crystals. By increasing the flow rate of the carrier gas, we successfully reduced the crystal size of ZnPc NWs and stabilized the α-form ZnPc NW crystals, which enabled the growth of high-yield α-form ZnPc NWs very selectively. In particular, the α-form ZnPc NWs grown at a carrier gas flow rate of 2000 sccm show extremely high water dispersibility without any significant aggregation after dispersion in water for 8 h.

Materials and methods

Synthesis of ZnPc and CuPc NWs

ZnPc NWs and CuPc NWs were prepared using commercially available zinc phthalocyanine (ZnPc, 97%, Sigma–Aldrich) and copper phthalocyanine (CuPc, 97%, Sigma–Aldrich) precursors, respectively, without further purification. Approximately 20 mg of precursor loaded in a ceramic boat was placed at the center of a tube furnace using a quartz protection tube. We placed a piece of Si (100) substrate at the end region of the quartz tube where the temperature naturally decreased to less than 80 °C to collect the resulting crystals effectively. After flushing the quartz tube using Ar gas at a flow rate of 1000 sccm for 5 min, we increased the furnace temperature up to 500 °C under specific Ar flow rates (50, 200, 800, 2000 sccm). After 10 min of reaction at the target temperature, the furnace was cooled naturally to room temperature by turning the power of the furnace off.

Characterization of ZnPc and CuPc NWs

The morphology of the resulting crystals was analyzed by scanning electron microscopy (SEM, JSM-7401F, JEOL). To prevent electron charging of the crystals, a platinum coating was applied to create a conductive layer on the crystal surface. Additionally, X-ray diffraction patterns of ZnPc and CuPc crystals were obtained from the 5D beamline at the Pohang Accelerator Laboratory (PAL). All obtained data were converted to the wavelength of CuKα (λ (K1.541841 Å) for better comparison with references. High-resolution transmission electron microscopy (HRTEM, JEM-2200FS, JEOL) was performed for structure analysis, and the samples for TEM measurements were prepared by stamping the ZnPc crystals onto a carbon-coated Cu grid.

Preparation and quantitative analysis of dispersed solutions

For the quantitative analysis of α-form ZnPc crystals obtained at different flow rates, we used a standard calibration method using distinctive light absorption bands of α-form ZnPc measured by a UV-VIS spectrometer (UV-2600, SHIMADZU). To obtain a standard calibration curve between the concentration and absorbance of α-form ZnPc, only α-form ZnPc dispersed aqueous solutions were prepared as follows:

ZnPc NW dispersed aqueous solutions were prepared by dissolving ZnPc crystals obtained by the PVT method in deionized (DI) water, followed by 40 min of sonication (Fig. S1a). After 24 h, the upper (well-dispersed α-form) part of the ZnPc NW solution was isolated, and α-form ZnPc was obtained in powder form by vacuum drying of the isolated solution. Using powder X-ray diffraction (PXRD) and UV-VIS results, we confirmed that the resulting product was α-form ZnPc (Fig. S1c and d). The obtained pure α-form ZnPc was redispersed in water and sequentially diluted to obtain reference solutions with five different α-form ZnPc concentrations (Fig. S1b). The absorption intensity of the reference solutions increased according to the α-form ZnPc concentration (Fig. S1d). The concentration and absorbance showed a linear relationship, as shown in Fig. S1e.

Based on these reference data, the concentration of α-form ZnPc in each solution obtained at different flow rates was determined by measuring the optical absorbance at 785 nm of the upper (well-dispersed) part of the 8-h-stored ZnPc solution. By matching the absorbance of the solution of interest with the reference linear fitting data represented in Fig. S1e, the weight percent of α-form ZnPc in each flow rate condition was calculated by multiplying the concentration of α-form ZnPc by the volume of water.

Results and discussion

To obtain high-yield and high-quality α-form ZnPc NWs, we used the PVT method, which employs vaporization, condensation and recrystallization processes of target precursor molecules.[10,21] Briefly, ZnPc powder located in the center of a tube furnace was vaporized at 500 °C, and Ar gas was used as a carrier gas to deliver

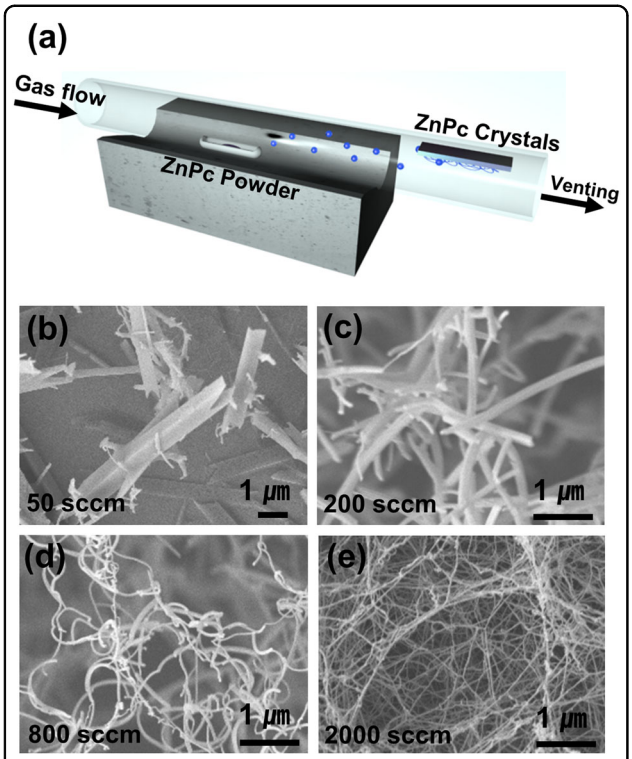

Fig. 1 Experimental scheme and morphologies of ZnPc crystals grown at different flow rates. a Schematic view of the PVT system used to grow ZnPc crystals. SEM images of ZnPc crystals grown at carrier gas flow rates of **b** 50 sccm, **c** 200 sccm, **d** 800 sccm and **e** 2000 sccm.

ZnPc vapors to a cooler region. A silicon substrate was placed at the end region of the furnace where the temperature naturally decreased to collect resulting crystals efficiently (Fig. 1a). After 10 min of reaction, blue ZnPc crystals were formed at the end of the tube furnace.

The preferred formation of α- and β-form ZnPc crystals depends on the crystal size due to their lattice potentials and surface energies.[18] According to the Buckingham equation used for estimating the interatomic nonbonding potentials in organic molecular crystals, α-form ZnPc is more stable than the β-form when the crystal size is small.[18] Normally, in the case of the vapor-phase deposition process, the crystal size is highly affected by the flow rate of the carrier gas.[21,22] Therefore, we varied the flow rate of Ar gas from 50 to 2000 sccm to evaluate the effect of carrier gas flow rate on the selection of the ZnPc structure. Figure 1b–e shows SEM images of ZnPc crystals obtained at different flow rates of Ar gas. As the flow rate increased, the width of the crystals decreased from approximately 500 nm (at 50 sccm (Fig. 1b)) to 50 nm (at 2000 sccm (Fig. 1e)). To confirm the crystal structures, we performed the PXRD and high-resolution transmission electron microscopy (HR-TEM). For clear observation of each diffraction peak, the intensity of the

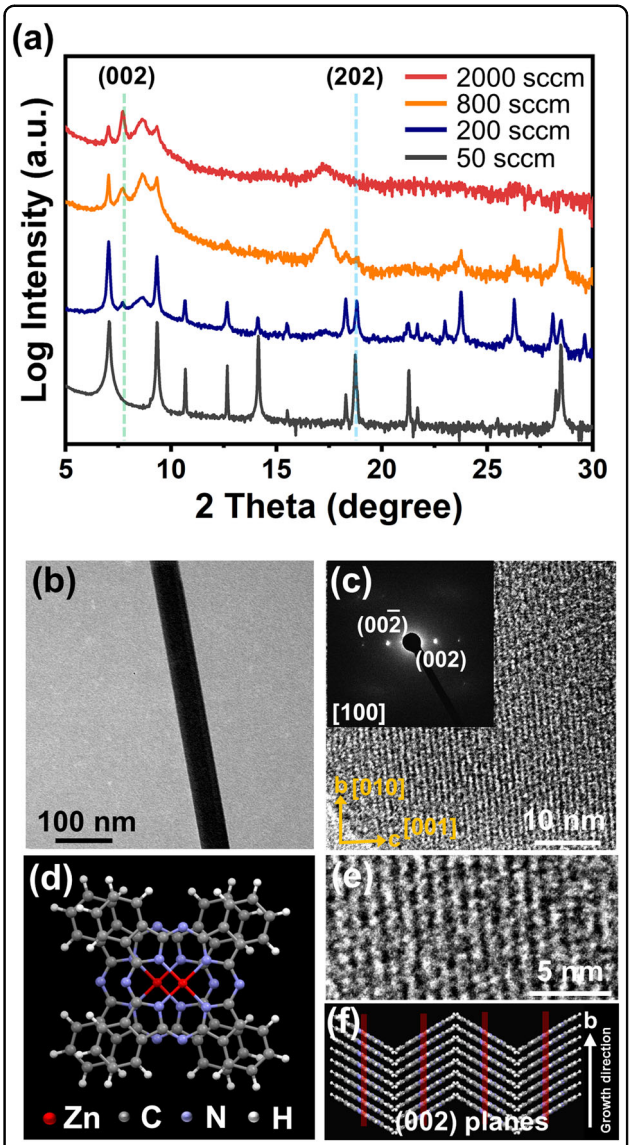

Fig. 2 Crystal structure analysis of α-form ZnPc NW crystals. a PXRD patterns of ZnPc NW crystals grown at different flow rates. **b** Low-magnification TEM image and **c** high-resolution TEM (HR-TEM) image of the α-form ZnPc NW. The inset shows the ED pattern of the ZnPc NW with [100] projection. **d** Stacking arrangement of the α-form ZnPc crystal along the normal of the planar molecule. **e** Magnified image of **c**. **f** Schematic view of the successive stacking of ZnPc molecules on the [100] projection.

PXRD patterns represented in Fig. 2a was converted from a linear scale to a logarithmic scale. The PXRD patterns plotted on a linear scale are represented in Fig. S2. Figure 2a shows the PXRD patterns of the resulting crystals grown at different flow rates. Due to the different packing structures of α- and β-form ZnPc crystals, different characteristic X-ray diffraction patterns were obtained. One of the representative characteristic diffraction planes of the α- and β-forms of ZnPc crystals are the (002) and

(202) planes, which show diffraction peaks at $2\theta = 7.712°$ and $2\theta = 18.783°$, respectively.[23–26] In the case of ZnPc crystals grown at a flow rate of 50 sccm (black line in Fig. 2a), a diffraction peak attributed to the (202) plane of the β-form is clearly observed, while that attributed to the (002) plane of the α-form is absent, which implies that β-form ZnPc crystals are dominantly obtained at relatively low carrier gas flow rates. Furthermore, the (202) diffraction peak of the β-form gradually decreased while a new (002) peak of the α-form appeared as the flow rate increased. At a flow rate of 2000 sccm (red line in Fig. 2a), we observed a clear (002) diffraction peak from the α-form and a disappearance of the (202) diffraction peak from the β-form, which means that α-form ZnPc crystals are selectively grown at a relatively high flow rate. These results show that the crystal phase of ZnPc can be successfully controlled by changing the flow rate of the carrier gas in the PVT method. Furthermore, we tried to analyze several peaks in the XRD data based on the JC-PDS database. The peaks that appeared at ~7.0° in both α- and β-form ZnPc were difficult to distinguish due to the small difference in the two-theta values of the (200) plane of the α-form and $(\bar{1}01)$ plane of the β-form, with peaks appearing at 6.8° and 7.0°, respectively.[23–26] Additionally, the peaks appearing at 23.7° and 26.2° are consistent with the (211) and (212) planes of β-form ZnPc, respectively.[23–26] The absence of two peaks at a flow rate of 50 sccm was due to relatively well-defined and homogeneous exposed crystal facets (Fig. 1b) compared to other ZnPc crystals obtained at flow rates of 200 and 800 sccm, of which the exposed planes were inhomogeneous and random due to their cylindrical wire morphology (Fig. 1c, d).

The characteristic crystal planes of α- and β-form ZnPc crystals were also confirmed using TEM measurements. Figure 2b shows a low-magnification image of an α-form ZnPc NW that has a uniform surface with a width of ~50 nm and a length of a few micrometers. The width of the thinnest NW obtained at a flow rate of 2000 sccm was ~12 nm (Fig. S3). Additionally, Fig. 2c and e show HR-TEM images of the α-form ZnPc NW shown in Fig. 2b, which show well-defined crystalline planes. The inset in Fig. 2c shows an electron diffraction (ED) pattern of a NW with clear diffraction spots having a lattice distance of 1.134 nm, which is consistent with the distance between the (002) planes observed in the PXRD pattern in Fig. 2a ($d_{(002)} = 11.464$ Å at $2\theta = 7.712°$). Figure 2e shows a magnified image of the (002) lattice that corresponds to the aligned Zn ions, as represented by the red lines in Fig. 2f, which shows growth of ZnPc NWs along the [010] direction stacked by π-π interactions. Figure 2d shows a molecular structure with a detailed stacking arrangement of α-form ZnPc along the normal of the planar molecule. The largest difference in the molecular packing structure between α- and β-form ZnPcs is the angle between the normal of the planar ZnPc molecule and the column direction (b axis).[18] Due to the small angle of α-form ZnPc (≈25°) compared to the β-form (≈45°), the zinc and nitrogen atoms of α-form ZnPc NWs have available bonding sites that can interact with water molecules through coordination and hydrogen bonds.[3] On the other hand, water molecules cannot interact with β-form ZnPc because Zn(II) ions and nitrogen atoms form coordination bonds to adjacent ZnPcs.[3] To confirm the detailed crystal structure of the β-form ZnPc NWs, we also obtained HR-TEM images and ED patterns (Fig. S4). The lattice distance of the (202) plane of the β-form is 0.480 nm, which matches well with our PXRD results ($d_{(202)} = 4.724$ Å at $2\theta = 18.783°$) in Fig. 2a. From the crystal structure analysis, we confirmed the relationship between the crystal phase and carrier gas flow rate, which became the key for the selective growth of α-form ZnPc. Additionally, a phase diagram of the ZnPc NW indicating its phase transformation according to its size was generated by measuring the crystal size and corresponding phases of the ZnPc NW by TEM analysis (Fig. S5c). The width of ZnPc NWs was determined from the TEM images, and the phase of ZnPc NWs was identified from the ED patterns. The experimentally measured largest width of the α-form and the smallest width of the β-form were 143 nm and 172 nm, respectively (Fig. S5a and b). Figure S5c displays a phase diagram showing the range of critical size for phase transformation, 140 ~ 170 nm, of which statistical data were obtained by measuring 37 different ZnPc NWs. These results were well matched with a reference paper that suggests the critical size for the phase transformation of ZnPc films to be 100 ~ 150 nm experimentally and 200 ~ 300 nm by calculations.[16]

The most remarkable property of the selectively grown α-form ZnPc NWs is the drastically improved water dispersibility. To confirm the water dispersibility of ZnPc crystals obtained at different flow rates, the same amount of each product was examined by dispersing the material in DI-water and monitoring any precipitate for a designated time. The top row of Fig. 3a shows a photograph of the solutions obtained after 40 min of ultrasonication to disperse α-form ZnPc NWs uniformly. Except for the leftmost solution prepared using ZnPc crystals obtained at a flow rate of 50 sccm, which is pale blue, the other solutions show a similar darker blue color. After 8 h of storage under ambient conditions, the ZnPc solution of the crystals obtained at a flow rate of 50 sccm shows severe precipitation, while as the flow rate increases, the precipitation decreases significantly (the bottom row of Fig. 3a). In particular, the solution of the ZnPc crystals obtained at a flow rate of 2000 sccm (rightmost side of Fig. 3b) shows a highly improved water dispersibility

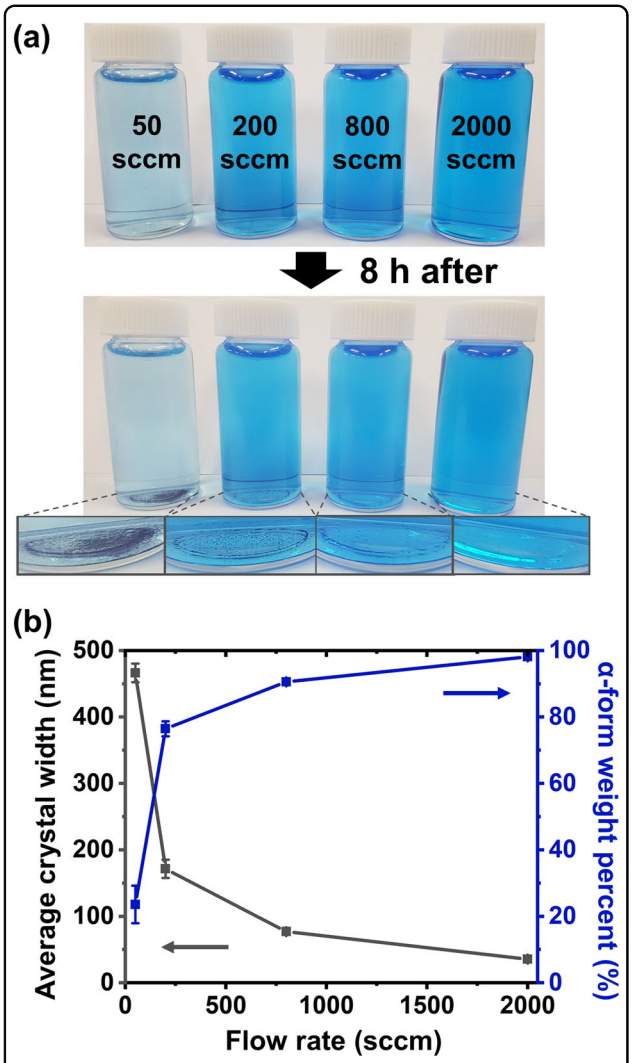

Fig. 3 Water dispersibility test and statistical study of obtained ZnPc crystals according to the flow rate. a Photographs of ZnPc crystals dispersed in water depending on the flow rate of carrier gas. **b** Tendency of the statistical width and α-form weight percent of the ZnPc crystals grown at different flow rates.

without significant precipitation. These results agree well with the PXRD data that show an increased ratio of α-form ZnPc as the flow rate of the carrier gas increased.

For the quantitative analysis of α-form ZnPc NW solutions, we obtained UV-VIS spectra of the solutions after removing the precipitates (β-form ZnPc). Based on the characteristic absorption peak of α-form ZnPc that appeared at 785 nm, the weight percentage of α-form ZnPc in the solution was calculated by comparing the peak intensity with the absorption spectrum of the reference solutions (Fig. S1). As expected from the PXRD data (Fig. 2a), the calculated weight percent of α-form ZnPc in the product increased as the flow rate of the carrier gas increased (blue line in Fig. 3b). Additionally, to our surprise, the percentage of the α-form reached over 98% at a flow rate of 2000 sccm. The black line in Fig. 3b shows the relationship between the flow rate and average width of ZnPc NW crystals, which decreases as the flow rate increases from 460 nm (50 sccm) to 35 nm (2000 sccm). By comparing and analyzing three important values, i.e., average width, weight percent of α-form ZnPc NWs and flow rate of the carrier gas, we clearly confirmed that α-form ZnPc NWs were favorably grown at a high carrier gas flow rate, by which the width of the NWs was effectively reduced.

To confirm the versatility of our strategy, we tried to control the phase of copper phthalocyanine (CuPc), which is well known as a good hole injection material for light-emitting diodes.[27,28] Due to the low solubility of this material in water and other organic solvents, uniform coating of CuPc on the target substrate is one of the major hurdles for device applications.[29,30] Therefore, we controlled the flow rate of the carrier gas to reduce the size of the CuPc crystals to improve their water dispersibility. Similar to ZnPc, CuPc was formed into a nanowire-shaped morphology, and the width of the CuPc NWs was successfully reduced by increasing the flow rate of the carrier gas (Fig. S6). When we dispersed the resulting CuPc NWs obtained at each flow rate condition in water, CuPc NWs grown at a high flow rate exhibited a higher water dispersibility (Fig. S7). Additionally, we verified that the metastable form of CuPc was dominantly grown at a relatively high flow rate, while the stable β-form of CuPc was mainly grown at a relatively low flow rate through PXRD analysis (Fig. S8). From these results, we convince that our flow rate-controlled PVT method would be applicable to various Pc crystals.

Conclusions

We successfully obtained a high yield of α-form ZnPc NWs that show outstanding water dispersibility without aggregation or significant precipitation. The selective growth of α-form ZnPc NWs was achieved by simply controlling the flow rate of the carrier gas in the PVT method. Through morphology observation and crystal structure analysis, we proved that the width of ZnPc crystals was successfully controlled by changing the flow rate of the carrier gas, which affects the selection of the crystal phase of ZnPc. Through UV-VIS analysis, we confirmed that more than 98% of the ZnPc crystals were α-form ZnPc. Our findings proved that flow rate control during the PVT process could be an effective way to obtain kinetically favorable ZnPc crystals with a specific phase. We believe that our results will contribute to the understanding of the crystallization of molecules, especially in terms of crystal structure control, and offer a great opportunity for various Pcs for their practical applications in aqueous solution form.

Acknowledgements
The authors acknowledge funding from the Veteran Researcher Grant (No. 2019R1A2C2004259) managed by the National Research Foundation of Korea (NRF) and Samsung Electronics. For the structure analysis, powder X-ray diffraction patterns were obtained at the 5D beamline of the Pohang Accelerator Laboratory (PAL, South Korea). Morphology and crystal structure observations of ZnPc NWs were carried out using HR-TEM at the National Institute for Nanomaterials Technology (NINT) in Pohang, South Korea.

Conflict of interest
The authors declare that they have no conflict of interest.

Publisher's note
Springer Nature remains neutral with regard to jurisdictional claims in published maps and institutional affiliations.

Supplementary information is available for this paper at https://doi.org/10.1038/s41427-020-0198-7.

Received: 15 November 2019 Revised: 23 December 2019 Accepted: 25 December 2019.
Published online: 7 February 2020

References

1. Wang, X., Garcia, T., Monaco, S., Schatschneider, B. & Marom, N. Effect of crystal packing on the excitonic properties of rubrene polymorphs. *CrystEngComm* **18**, 7353–7362 (2016).
2. Law, K. Y. Organic photoconductive materials: recent trends and developments. *Chem. Rev.* **93**, 449–486 (1993).
3. Moon, H. K. et al. Significant increase in the water dispersibility of zinc phthalocyanine nanowires and applications in cancer phototherapy. *NPG Asia Mater.* **4**, e12 (2012).
4. Zhen, Y. G., Dong, H. L., Jiang, L. & Hu, W. P. Tailoring crystal polymorphs of organic semiconductors towards high-performance field-effect transistors. *Chin. Chem. Lett.* **27**, 1330–1338 (2016).
5. He, T. et al. Single-crystal field-effect transistors of new Cl2-NDI polymorph processed by sublimation in air. *Nat. Commun.* **6**, 5954 (2015).
6. Li, X., Xiao, Y., Wang, S. & Li, X. Ultra-photosensitive Y-type titanylphthalocyanine nanocrystals: preparation and photoelectric properties. *Dye. Pigment.* **125**, 44–53 (2016).
7. Weiss, D. S. & Abkowitz, M. Advances in organic photoconductor technology. *Chem. Rev.* **110**, 479–526 (2010).
8. Desiraju, G. R. Cryptic crystallography. *Nat. Mater.* **1**, 77–79 (2002).
9. Zhao, X., Bao, Z., Sun, C. & Xue, D. Polymorphology formation of Cu2O: a microscopic understanding of single crystal growth from both thermodynamic and kinetic models. *J. Cryst. Growth* **311**, 711–715 (2009).
10. Park, C., Park, J. E. & Choi, H. C. Crystallization-induced properties from morphology-controlled organic crystals. *Acc. Chem. Res.* **47**, 2353–2364 (2014).
11. Martí-Rujas, J. & Kawano, M. Kinetic products in coordination networks: Ab initio X-ray powder diffraction analysis. *Acc. Chem. Res.* **46**, 493–505 (2013).
12. Zhang, Z. et al. The impact of interlayer electronic coupling on charge transport in organic semiconductors: a case study on titanylphthalocyanine single crystals. *Angew. Chemie Int.* **55**, 5206–5209 (2016).
13. He, P. et al. Tuning the crystal polymorphs of alkyl thienoacene via solution self-assembly toward air-stable and high-performance organic field-effect transistors. *Adv. Mater.* **27**, 825–830 (2015).
14. Vasseur, K. et al. Correlating the polymorphism of titanyl phthalocyanine thin films with solar cell performance. *J. Phys. Chem. Lett.* **3**, 2395–2400 (2012).
15. Wang, K. et al. Organic polymorphs: one-compound-based crystals with molecular-conformation- and packing-dependent luminescent properties. *Adv. Mater.* **26**, 6168–6173 (2014).
16. Vergnat, C., Landais, V., Legrand, J. F. & Brinkmann, M. Orienting semiconducting nanocrystals on nanostructured polycarbonate substrates: impact of substrate temperature on polymorphism and in-plane orientation. *Macromolecules* **44**, 3817–3827 (2011).
17. Löbbert, G. in *Ullmann's Encycl. Ind. Chem.* **27**, 181–213 (Wiley-VCH Verlag GmbH & Co. KGaA, 2000).
18. Iwatsu, F. Size effects on the alpha-beta transformation of phthalocyanine crystals. *J. Phys. Chem.* **92**, 1678–1681 (1988).
19. Fryer, J. R., McKay, R. B., Mather, R. R. & Sing, K. S. W. The technological importance of the crystallographic and surface properties of copper phthalocyanine pigments. *J. Chem. Technol. Biotechnol.* **31**, 371–387 (1981).
20. Belenguer, A. M. et al. Understanding the influence of surface solvation and structure on polymorph stability: a combined mechanochemical and theoretical approach. *J. Am. Chem. Soc.* **140**, 17051–17059 (2018).
21. Yoon, S. M. et al. Vaporization-condensation-recrystallization process-mediated synthesis of helical m-aminobenzoic acid nanobelts. *Langmuir* **23**, 11875–11882 (2007).
22. Ullah, A. R., Micolich, A. P., Cochrane, J. W. & Hamilton, A. R. The effect of temperature and gas flow on the physical vapour growth of mm-scale rubrene crystals for organic FETs. *Device Process Technol. Microelectronics MEMS Photonics Nanotechnol. IV* **6800** 680005 (2007).
23. Senthilarasu, S. et al. Characterization of zinc phthalocyanine (ZnPc) for photovoltaic applications. *Appl. Phys. A Mater. Sci. Process* **77**, 383–389 (2003).
24. Iwatsu, F. Crystal behavior of zinc phthalocyanine films in alcohols. *J. Cryst. Growth* **71**, 629–638 (1985).
25. Zeyada, H. M. & El-Nahass, M. M. Electrical properties and dielectric relaxation of thermally evaporated zinc phthalocyanine thin films. *Appl. Surf. Sci.* **254**, 1852–1858 (2008).
26. Senthilarasu, S., Hahn, Y. B. & Lee, S.-H. Structural analysis of zinc phthalocyanine (ZnPc) thin films: X-ray diffraction study. *J. Appl. Phys.* **102**, 043512 (2007).
27. Yu, W.-L., Pei, J., Cao, Y. & Huang, W. Hole-injection enhancement by copper phthalocyanine (CuPc) in blue polymer light-emitting diodes. *J. Appl. Phys.* **89**, 2343–2350 (2001).
28. Li, L., Guan, M., Cao, G., Li, Y. & Zeng, Y. Low operating-voltage and high power-efficiency OLED employing MoO 3-doped CuPc as hole injection layer. *Displays* **33**, 17–20 (2012).
29. Tianyong, Z. & Chunlong, Z. Properties of copper phthalocyanine blue (C.I. Pigment Blue 15:3) treated with poly(ethylene glycol)s. *Dye. Pigment.* **35**, 123–130 (1997).
30. Ghani, F., Kristen, J. & Riegler, H. Solubility properties of unsubstituted metal phthalocyanines in different types of solvents. *J. Chem. Eng. Data* **57**, 439–449 (2012).